Hematopoietic-SLC37A2 deficiency impairs M2 macrophage polarization and accelerates atherosclerosis in LDL receptor-deficient mice

Qingxia Zhao[1, 5], Zhan Wang[1, 5], Allison K. Meyers[2], Jennifer Madenspacher[3], Manal Zabalawi[1], Elena Boudyguina[1], Fang-Chi Hsu[4], Charles M. McCall[1, 2], Cristina M. Furdui[1], John S. Parks[1], Michael B. Fessler[3], Xuewei Zhu[1, 2, 6]

[1.] Department of Internal Medicine, Section on Molecular Medicine, Wake Forest School of Medicine, Winston-Salem, NC 27157, USA

[2.] Department of Microbiology and Immunology, Wake Forest School of Medicine, Winston-Salem, NC 27157, USA

[3.] Immunity, Inflammation and Disease Laboratory, National Institute of Environmental Health Sciences, NIH, Research Triangle Park, NC 27709, USA

[4]. Department of Biostatistics and Data Science, Wake Forest School of Medicine, Winston-Salem, NC, USA

[5]. These authors contributed equally to this work.

[6]. Correspondence: Dr. Xuewei Zhu, Department of Internal Medicine, Section on Molecular Medicine, Wake Forest School of Medicine, Medical Center Blvd, Winston-Salem, NC 27157, USA; Phone: 336-713-1445; Fax: 336-716-6279; Email: xwzhu@wakehealth.edu

Conflict of interest statement: The authors declare no competing interests.

Abstract

Macrophages play a central role in the pathogenesis of atherosclerosis. Our previous study demonstrated that solute carrier family 37 member 2 (SLC37A2), an endoplasmic reticulum-anchored phosphate-linked glucose-6-phosphate transporter, negatively regulates macrophage Toll-like receptor activation by fine-tuning glycolytic reprogramming *in vitro*. However, whether macrophage SLC37A2 impacts *in vivo* macrophage inflammation and atherosclerosis under hyperlipidemic conditions is unknown. We generated hematopoietic cell-specific SLC37A2 knockout and control mice in C57Bl/6 Ldlr$^{-/-}$ mice by bone marrow transplantation. Hematopoietic-specific SLC37A2 deletion in Ldlr$^{-/-}$ mice increased plasma lipid concentrations 12-16 wks of Western diet induction, attenuated M2 macrophage activation, and resulted in more atherosclerosis compared to Ldlr$^{-/-}$ mice transplanted with wild type bone marrow. Aortic root intimal area was inversely correlated with plasma IL-10 levels, but not total cholesterol concentrations, suggesting macrophage polarization but not plasma cholesterol was responsible for increased atherosclerosis in bone marrow SLC37A2-deficient mice. SLC37A2 deficiency also impaired macrophage M2 activation induced by IL-4 or apoptotic cells *in vitro*. In conclusion, our study suggests that SLC37A2 expression is required to support macrophage M2 polarization *in vitro* and *in vivo*. *In vivo* disruption of hematopoietic SLC37A2 accelerates atherosclerosis under hyperlipidemic pro-atherogenic conditions.

Introduction

Cardiovascular disease, caused mainly by atherosclerosis, is a leading cause of mortality worldwide (1). Atherosclerosis is driven by hyperlipidemia and exacerbated by chronic low-grade inflammation (2-7). Macrophages are among the most abundant immune cells within atherosclerotic plaques (2, 6, 8-11). Hyperlipidemia drives circulating Ly6C^{high} monocytes to migrate into the artery wall, where they differentiate into macrophages. Lesional macrophages can also develop from resident macrophage proliferation in the local artery tissues (12). Atherosclerotic plaque macrophages take up modified LDL (i.e., oxidized LDL; oxLDL), forming lipid laden-macrophages or foam cells. Foam cell accumulation contributes to inflammation and atherosclerotic plaque growth (2, 6, 8-11).

Macrophages are heterogeneous but can be generally grouped into two categories based on their inflammatory activities: classically activated M1-type macrophages and alternatively activated M2-type macrophages. M2 macrophages can be further subdivided into M2a, 2b, 2c, and 2d based on the stimuli and resultant transcriptional changes (13). The phenotypic shift between M1 and M2 activation significantly impacts atherosclerotic lesion progression and regression (2, 14, 15). For example, increased M1 macrophages in the atherosclerotic plaques promote inflammation, cell death, and necrotic core formation, consequently accelerating atherosclerosis. Conversely, increased M2 macrophages in atherosclerotic plaques promote apoptotic cell clearance and resolution of inflammation, attenuating atherosclerosis. Therefore, uncovering the underlying mechanisms governing activation and deactivation of M1 or M2 macrophages and their phenotypic switch provides a promising avenue to prevent and treat atherosclerosis.

Activation and deactivation of macrophages rewire intracellular metabolic pathways, which in turn modify their cellular function (16-18). M1 macrophages require glycolysis and glucose utilization to mount an effective pro-inflammatory response. However, whether glycolytic reprogramming is necessary for M2 macrophage activation is still debatable and requires further investigation. Moreover, little is known about

how and to what extent macrophages reprogram cellular metabolism in response to microenvironmental stimuli to promote or resolve inflammation under pro-atherogenic conditions. A positive association between glycolysis and plaque macrophage inflammation was documented as increased glucose metabolic activity in human symptomatic and unstable plaque macrophages compared with asymptomatic lesions (19). However, macrophage glycolytic rate does not always influence atherogenesis, at least based on animal studies. For example, myeloid deletion of glucose transporter 1 (GLUT1), the primary glucose transporter on the plasma membrane in macrophages, does not alter atherosclerotic plaque size or macrophage content in $Ldlr^{-/-}$ mice (20). Moreover, myeloid overexpression of GLUT1 increases glucose flux in macrophages and enhances macrophage inflammation *in vitro* but is insufficient to promote atherosclerosis (21). These findings suggest a context-dependent regulation of macrophage inflammation and disease development by cellular metabolic processes in acute vs. chronic low-grade inflammation.

Solute carrier family 37 member 2 (SLC37A2) is an endoplasmic reticulum-anchored phosphate-linked glucose-6-phosphate transporter that is highly expressed in macrophages (22-24). We have recently reported that SLC37A2 plays a pivotal role in murine macrophage inflammatory activation and cellular metabolic rewiring (25). SLC37A2 deletion reprograms macrophages to a hyper-glycolytic state of energy metabolism and accelerates LPS-induced inflammatory cytokine production, partially depending on nicotinamide adenine dinucleotide (NAD^+) biosynthesis. Blockade of glycolysis or the NAD^+ salvage pathway normalizes the differential expression of pro-inflammatory cytokines between control and SLC37A2-deficient macrophages. Conversely, overexpression of SLC37A2 lowers macrophage glycolysis and significantly reduces LPS-induced pro-inflammatory cytokine expression. Our published work suggests that SLC37A2 is a negative regulator of murine macrophage M1 activation by down-regulating glycolytic reprogramming.

Despite these findings, it remains unclear whether macrophage SLC37A2 impacts macrophage M1/M2 polarization *in vivo* under pathologic conditions. Further, it is not known whether macrophage SLC37A2-mediated inflammation affects the pathogenesis of inflammatory diseases. In this study, we demonstrate that SLC37A2 expression is necessary to maintain M2 macrophage activation *in vitro* and *in vivo*. Disruption of hematopoietic SLC37A2 worsens hyperlipidemic-induced atherosclerosis, primarily by impairing M2 macrophage polarization.

Results

Hematopoietic SLC37A2 deletion increases plasma lipids in WD-fed Ldlr$^{-/-}$ mice

We previously showed that SLC372 is a novel regulator of macrophage inflammation by controlling glycolysis. In this study, we wanted to know whether mice lacking SLC37A2 in macrophages were at an increased risk of developing atherosclerosis. To do this, we generated hematopoietic SLC37A2 knockout (SLC37A2$^{\Delta hema}$) and control mice by transplanting bone marrow from female SLC37A2KO and wild type (WT) mice into irradiated male Ldlr$^{-/-}$ mice. After 5 wks of recovery, the mice were switched from a standard laboratory diet to a high-fat Western diet (WD) for 16 wks to promote the development of advanced atherosclerosis. The bone marrow transplantation efficiency was ~90% based on the male Sry gene expression in blood leukocytes isolated from recipient mice examined after 16-wk WD feeding (**Supplemental Figures 1A** and **1B**). Periodic measurements of total plasma cholesterol (TPC), free cholesterol (FC), cholesteryl ester (CE), and triglyceride (TG) levels were conducted during disease progression (**Figures 1A-1D**). Chow-fed (i.e., baseline) control and SLC37A2$^{\Delta hema}$ mice displayed similar plasma lipid concentrations. Four wks of WD feeding increased plasma lipid (including TPC, FC, CE, and TG) concentrations in both genotypes. Interestingly, SLC37A2$^{\Delta hema}$ mice displayed significantly higher plasma cholesterol (TPC, FC, and CE) concentrations after 12 and 16 wks of diet feeding (**Figures 1A-1C**). SLC37A2$^{\Delta hema}$ mice also showed significantly higher plasma TG concentration after 16 wks of diet feeding (**Figure 1D**). Furthermore, we observed significantly higher plasma VLDL and LDL cholesterol concentrations but only a marginal increase in HDL cholesterol in SLC37A2$^{\Delta hema}$ vs. WT mice after 16 wks of diet feeding, analyzed by fasting protein liquid chromatography fractionation of plasma (**Figure 1E**). Collectively, these results suggest a novel role for hematopoietic SLC37A2 in lipid metabolism under pro-atherogenic conditions.

Hematopoietic SLC37A2 deletion increases liver CE and reduces hepatic M2 macrophage activation in WD-fed Ldlr$^{-/-}$ mice

Given the increased plasma lipid concentrations in high-fat WD-fed SLC37A2$^{\Delta hema}$ mice, we next measured liver lipid concentrations. Consistent with increased plasma lipid concentrations, we observed a significant increase in hepatic TC and CE, but not FC or TG in SLC37A2$^{\Delta hema}$ vs. WT mice (**Figure 2A**). The increased plasma and liver lipid concentrations in SLC37A2$^{\Delta hema}$ mice prompted us to examine the hepatic expression of genes involved in lipid metabolism in diet-fed mice. As expected, Slc37a2 transcript was significantly lower in SLC37A2$^{\Delta hema}$ mice receiving bone marrow from SLC37A2KO mice, indicating the success of BMT (**Figure 2B**). We found that hepatic expression of genes responsible for de novo lipogenesis was similar between genotypes of mice (**Figure 2C**). There was a slightly but significantly decreased expression of cholesterol transporter protein ABCA1 (**Figure 2C**). Interestingly, hepatic expression of the receptor for fatty acid uptake (CD36), enzymes for fatty acid oxidation (Cpt1a, Acox1, Acadl), and transcriptional factors and coactivators regulating fatty acid oxidation (PGC1α, PGC1β, PPARδ, and PPARγ) were all down-regulated in SLC37A2$^{\Delta hema}$ vs. WT liver (**Figure 2D**), suggesting an impaired fatty acid utilization in SLC37A2$^{\Delta hema}$ mouse liver at least at the transcriptional level. Because alternative activation of hepatic macrophages promotes liver fatty acid oxidation and improves metabolic syndrome (26), we next examined macrophage M1 and M2 activation states by measuring hepatic gene expression of macrophage markers, M1-type cytokines, and chemokines, and M2 macrophage markers. Different from our *in vitro* study, in which we observed increased pro-inflammatory cytokine production in SLC37A2$^{\Delta hema}$ macrophages in response to TLR activation, under pro-atherogenic conditions, hematopoietic SLC37A2 deficiency has a minor effect on the expression of genes encoding macrophage markers (**Figure 2E**) and pro-inflammatory cytokines and chemokines (**Figure 2F**) at the transcript level and protein level (**Figure 2G** and **2H**). Rather, we observed a decreased IL-6 transcript (**Figure 2F**) and IFN-γ and MCP-1 (**Figure 2G** and **2H**) protein concentration in SLC37A2$^{\Delta hema}$ liver, suggesting that SLC37A2 deletion in bone marrow is not sufficient to induce a pro-inflammatory response in the liver under pro-atherogenic conditions. Despite the equivalent or slightly decreased M1 cytokines/chemokines in SLC37A2$^{\Delta hema}$ liver, hepatic M2 macrophage markers, including Arg1, Mrc1, Ym1, and IL-10, showed

significantly lower expression in SLC37A2$^{\Delta hema}$ vs. WT liver (**Figure 2I**). Consistent with the decreased transcript expression, hepatic IL-10 protein concentration showed a trend toward a decrease in SLC37A2$^{\Delta hema}$ liver, relative to control (**Figure 2J**). Taken together, our results suggest that genetic deletion of SLC37A2 in bone marrow cells impairs alternative activation of hepatic macrophages, associated with lower hepatic fatty acid oxidation gene expression and increased liver lipid accumulation.

Hematopoietic SLC37A2 deletion impairs anti-inflammatory responses in WD-fed Ldlr$^{-/-}$ mice

To determine whether hematopoietic SLC37A2 deletion affects inflammation at the systemic level, we first examined plasma concentrations of pro-inflammatory cytokines, chemokines, and anti-inflammatory cytokine using a multiplex assay. Consistent with the expression pattern of hepatic cytokines and chemokines, plasma pro-inflammatory cytokine concentrations did not differ between genotypes (**Figure 3A**). But, plasma MCP-1 concentration was significantly lower in the SLC37A2$^{\Delta hema}$ vs. WT mice (**Figure 3B**). Strikingly, the SLC37A2$^{\Delta hema}$ mice displayed a 70% reduction of the anti-inflammatory cytokine IL-10 in plasma (**Figure 3C**) relative to their WT counterparts, suggesting hematopoietic SLC37A2 deletion impairs IL-10 production under pro-atherogenic conditions.

Consistent with the pro-inflammatory and anti-inflammatory cytokine profiles in liver and plasma, SLC37A2$^{\Delta hema}$ vs. WT mice showed indistinguishable expression of pro-inflammatory cytokines (**Figure 3D**) but significantly attenuated Arg1 and Mrc1 (M2 markers) expression in resident peritoneal macrophages (**Figure 3E)** after 16-wk diet feeding. Together, our results suggest that hematopoietic SLC37A2 deletion primarily impairs anti-inflammatory responses in Ldlr$^{-/-}$ mice when challenged with WD diet.

Hematopoietic SLC37A2 deletion has a minor effect on blood myeloid cell composition after 16-wks of diet feeding

As described above, deletion of SLC37A2 in bone marrow elevated plasma cholesterol concentration. Hypercholesterolemia drives blood monocytosis and neutrophilia by promoting myeloid progenitor cell proliferation in the bone marrow and spleen compartments. We next assessed whether hematopoietic SLC37A2 deletion affects monocyte and neutrophil composition in blood as well as in the spleen. **Supplemental Figure 2A** shows our flow cytometry gating strategies. At 9-wk WD feeding, no difference was observed between genotypes regarding the frequency of blood monocytes ($CD11b^{+}CD115^{+}$), $Gr1^{low}$ monocytes ($CD11b^{+}CD115^{+}Gr1^{low}$), $Gr1^{high}$ monocytes ($CD11b^{+}CD115^{+}$ $Gr1^{high}$), or neutrophils ($CD11b^{+}CD115^{-}Gr1^{+}$) (**Supplemental Figure 2B**), or the ratio of $Gr1^{low}$ and $Gr1^{high}$ monocytes in blood monocytes (**Supplemental Figure 2C**). After 16 wks of diet feeding, the percentage of blood neutrophils ($CD11b^{+}CD115^{-}Gr1^{+}$) was significantly increased in the $SLC37A2^{\Delta hema}$ mice (**Supplemental Figure 2D**). Despite the elevated plasma cholesterol and increased blood neutrophils, no difference was detected between genotypes in blood monocyte composition at 16-wk diet feeding (**Supplemental Figures 2D** and **2E**). We did not observe any significant changes in the monocyte and neutrophil composition in the spleen between genotypes (**Supplemental Figures 2F** and **2G**). Overall, these results suggest hematopoietic SLC37A2 deletion has a minimal effect on blood myeloid cell composition. Note that the concentration of plasma MCP-1, a primary chemokine recruiting monocytes and macrophages from bone marrow to circulation or from the blood circulation to tissues, was significantly lower in the $SLC37A2^{\Delta hema}$ mice (Figure 3B). We reason that the unaltered blood and spleen monocytes may be the net effect of the combination of decreased plasma MCP-1 and increased plasma cholesterol in the $SLC37A2^{\Delta hema}$ mice. Taken together, our results suggest that hematopoietic SLC37A2 deletion has a negligible effect on blood myeloid composition except for a slight increase in blood neutrophils after 16-wk WD feeding.

Hematopoietic SLC37A2 deficiency promotes atherosclerosis

Abnormal lipid metabolism and enhanced local and systemic inflammation accelerate atherosclerosis. Since we observed increased plasma lipids, especially apoB containing lipoproteins, and decreased IL-

10 in plasma, we next investigated the development of atherosclerosis in Slc37a2$^{\Delta hema}$ mice compared to controls. We found that hematopoietic SLC37A2-deficient mice showed larger aortic root lesions stained with Oil Red O (**Figures 4A-4B**), despite similar CD68 (macrophage marker) (**Figures 4C-4D**), suggesting that hematopoietic SLC37A2 deletion accelerates atherosclerotic plaque formation but has no effect on macrophage content. Additionally, hematopoietic SLC37A2 deletion also did not affect T cell content in the plaque, as shown by similar CD3 (T cell marker) staining between genotypes (**Supplemental Figure 3**). Since we observed increased plasma cholesterol, decreased plasma IL-10, and increased atherosclerosis in Slc37a2$^{\Delta hema}$ vs. control mice, we next assessed whether there is an association between plasma lipids vs. atherosclerosis or between plasma IL-10 vs. atherosclerosis in diet-fed mice by performing linear regression analysis. Despite no significant association between intimal area and plasma TC (**Figure 4E**), there was a significant inverse correlation between plasma IL-10 and intimal area (**Figure 4F**), suggesting that the impaired M2 activation or the attenuated anti-inflammatory response in the Slc37a2$^{\Delta hema}$ mice may be the primary driver of enhanced atherosclerosis in those mice.

IL-10 producing M2 macrophages is responsible for the engulfment and clearance of apoptotic cells (i.e., efferocytosis) (27). Failure of efferocytosis leads to pro-inflammatory and immunogenic consequences due to secondary necrosis, exaggerating atherosclerosis (28, 29). We examined necrotic core formation and quantified apoptosis and efferocytosis in the plaques. Compared to WT control, Slc37a2$^{\Delta hema}$ mice had a significant increase in necrotic area in aortic lesions (**Figure 4G and 4H**). However, no difference was observed regarding the frequency of apoptosis or efferocytosis in lesions between genotypes at 16 wks of diet feeding (**Figure 4I** and **4J**). Interestingly, when we stained the aortic root sections with Masson's Trichrome stain, we observed a significant reduction in Trichrome positive staining in Slc37a2$^{\Delta hema}$ vs. WT control aortic root sections (**Figure 4K** and **4L**), suggesting that hematopoietic SLC37A2 deficiency decreases collagen deposition, likely resulting from impaired M2 macrophage activation. As collagen formation is associates with the stability of plaques (30, 31), our data suggest that

SLC37A2 deficiency in bone marrow promotes plaque instability. Together, our results indicate that hematopoietic SLC37A2 deletion worsens atherosclerosis, which is inversely associated with plasma IL-10 levels.

Hematopoietic SLC37A2 deletion has minimal impact on insulin resistance and adipose inflammation under pro-atherogenic conditions

Chronic inflammation drives the progression of type 2 diabetes and insulin resistance. In addition to atherosclerosis assessment, we also tested whether hematopoietic SLC37A2 deletion influences adipose tissue inflammation and/or obesity and insulin resistance under pro-atherogenic conditions. WT and Slc37a2$^{\Delta hema}$ mice gained similar body weight over the 16 wks of diet feeding (**Supplemental Figure 4A**). Tissue (including liver, spleen, and epididymal fat) mass was comparable between genotypes (**Supplemental Figure 4B**). Both genotypic mice showed similar glucose clearance (measured by glucose tolerance test) and insulin tolerance (measured by insulin tolerance test) around 10 wks of diet feeding (**Supplemental Figure 4C** and **4D**). As expected, Slc37a2 mRNA expression was significantly reduced in the Slc37a2$^{\Delta hema}$ vs. control mouse epididymal fat. However, hematopoietic deletion of SLC37A2 did not alter adipose tissue inflammation, as quantified by qPCR analysis of gene expression of macrophage markers, M1 markers, and M2 markers, except for increasing ccr2 (MCP-1 receptor) expression (**Supplemental Figure 4E**). These results suggest that deletion of SLC37A2 in bone marrow cells has minimal impact on WD-induced obesity, insulin resistance, and adipose tissue under pro-atherosclerotic conditions.

OxLDL upregulates SLC37A2 protein expression and increases inflammation in SLC37A2-deficient macrophages *in vitro*

OxLDL contributes to atherosclerotic plaque formation by many different mechanisms. For instance, oxLDL promotes foam cell formation and triggers oxidative stress and pro-inflammatory responses in

macrophages (32, 33). Given that there was no significant increase in pro-inflammatory responses in Slc37a2$^{\Delta hema}$ vs. control mice after 16-wk WD feeding, we asked whether oxLDL can promote M1 activation in Slc37a2$^{-/-}$ macrophages *in vitro*. First, we examined SLC37A2 protein expression in BMDMs treated with or without oxLDL. oxLDL markedly increased SLC37A2 protein expression in BMDMs after 24 h stimulation (**Figure 5A**). oxLDL promoted cholesterol, particularly CE, accumulation in macrophages in a dose-dependent manner (**Figure 5B**), regardless of genotypes. However, SLC37A2 deletion does not affect cholesterol loading in macrophages (**Figure 5B**), suggesting a dispensible role of SLC37A2 in macrophage foam cell formation. Like LPS stimulated cells, Slc37a2$^{-/-}$ macrophages showed increased expression of Il-1β and Il-6, but not Tnf at the transcriptional level in response to 24 h of oxLDL stimulation (**Figure 5C**), suggesting that SLC37A2 is a stress-responsive protein and increased SLC37A2 expression likely serves as a protective mechanism for resolution of stress-induced inflammation.

SLC37A2 deficiency impairs IL-4-induced M2 macrophage activation

Our *in vivo* studies suggest that SLC37A2 is required to maintain macrophage M2 polarization under pro-atherogenic conditions. IL-4 signaling activates STAT6, which translocates into nuclei to induce expression of genes involved in fatty acid metabolism, including Cpt1a, Acox1, and Acodl, and transcriptional regulation (such as transcriptional factors PPARs and PPARγ coactivator PGC1β) for reprogramming macrophage lipid metabolism (34). The transcriptional synergy between STAT6, PPARs, and PGC-1 is necessary for the maximal expression of IL-4-induced M2 macrophage markers (35). To test whether SLC37A2 regulates IL-4 induced M2 polarization, we treated WT and SLC37A2-deficient BMDMs with 20 ng/ml IL-4 for 0, 6, and 24 h in RPMI-1640 medium containing 10% FBS and then examined IL-4 induced gene expression in macrophages. We found that IL-4 induced a 1.5 fold increase of Slc37a2 transcript at 6 h (**Figure 6A)** and a 2-fold increase of SLC37A2 protein at 24 h of stimulation (**Figure 6B**) in WT macrophages. Consistent with our *in vivo* findings, SLC37A2-deficient macrophages showed decreased expression of M2 markers, including Arg1, Mrc1, and Ym1 (**Figure 6C**), suggesting

that SLC37A2 expression is necessary for IL-4-induced macrophage M2 (M (IL-4)) polarization. Interestingly, SLC37A2 deletion also lowered MCP-1 expression in macrophages, consistent with the lower *in vivo* MCP-1 expression in diet-fed Slc37a2$^{\Delta hema}$ vs. control mice. However, IL-4 does not induce IL-10 expression in either genotypic macrophages, suggesting that M2 (IL-4) is not a major source of IL-10 in macrophages. Note that WT and SLC37A2- deficient macrophages displayed similar expression levels of metabolic regulators (**Figure 6D**) and fatty acid oxidation genes (**Figure 6E**), which are primarily regulated by STAT6 signaling, suggesting that SLC37A2 deficiency does not impair the STAT6 signaling. Together, our data suggest that SLC37A2 deficiency impairs M2 (IL-4) polarization, independent of PPARs and PGC1 expression.

Given that mitochondrial OXPHOS supports M2 (IL-4) macrophage activation (36), we next examined mitochondrial respiration by measuring oxygen consumption rate (OCR) in WT and SLC37A2KO BMDMs treated with or without 20 ng/ml IL-4 for 24 h. As expected, 24 h IL-4 stimulation promoted mitochondrial OXPHOS in WT macrophages, as shown by increased maximal OCR and spare respiratory capacity (**Figure 6F**). Interestingly, Slc37a2$^{-/-}$ vs. WT BMDMs displayed significantly higher basal respiration after 24 h of IL-4 stimulation (**Figure 6F** and **6G**). However, no genotypic difference was observed in maximal respiration or spare respiratory capacity in IL-4 treated cells, suggesting a minor impact of SLC37A2 deletion on mitochondrial OXPHOS in M2 (IL-4) macrophages. Additionally, evidence suggests that glycolysis and glucose utilization is required for M2 (IL-4) macrophage activation (36), while another study indicates that glycolysis is dispensible as long as mitochondrial OXPHOS is intact (37). Nevertheless, we next examined glycolysis by measuring extracellular acidification rate (ECAR) in WT and Slc37a2$^{-/-}$ BMDMs treated with or without 20 ng/ml IL-4 for 24 h. SLC37A2-deficient macrophages showed slightly increased glycolytic capacity at baseline. No difference in glycolysis or glycolytic capacity was observed between genotypes after IL-4 treatment. Overall, our results suggest that SLC37A2 deletion does not significantly impact glycolysis or mitochondrial OXPHOS in M2 (IL-4) macrophage. Thus, the attenuated

M2 (IL-4) activation in SLC37A2-deficient macrophages is likely independent of these two cellular metabolic processes.

SLC37A2 deficiency impairs apoptotic cell (AC)-induced M2 macrophage activation

As described above, one of the striking changes in the diet-fed Slc37a2$^{\Delta hema}$ vs. control mice is the 70% reduction of plasma IL-10, which is a major anti-inflammatory cytokine for cellular homeostasis. Macrophages are a major type of phagocytes that can produce a large amount of IL-10 in response to apoptotic cells (ACs) (38). The clearance of ACs and the suppression of inflammation by IL-10 are required to prevent chronic inflammation and reduce atherosclerosis progression. So, next, we examined apoptotic cell-induced M2 (M2 (AC)) activation in WT and SLC37A2-deficient macrophages. We first incubated Jurkat T cells with 1 μM staurosporine for 4 h to induce early apoptosis (Annexin V$^+$, PI$^-$). Under this condition, 60% of Jurkat T cells undergo apoptosis (**Supplemental Figure 5**). Compared to WT cells, SLC37A2-deficient macrophages showed a marked reduction in IL-10 expression at both transcriptional level (**Figure 7A**) and protein level (**Figure 7B**) in response to ACs. Engulfment of dead cells elevates macrophage fatty acids and mitochondrial β-oxidation, which supports NAD$^+$ homeostasis and IL-10 production (39). To explore the possible mechanisms of the attenuated M2 (AC) activation in SLC37A2-deficient macrophages, we first compared the efferocytosis index between genotypes. We found SLC37A2 deletion slightly enhanced engulfment of ACs over a 2-h period (**Figure 7C**). Blockade of phagocytosis by using cytochalasin D (**Figure 7D**) or blockade of fatty acid β-oxidation (**Figure 7E**) slightly reduced AC-induced IL-10 production in both genotypes, but did not normalize the differential expression of IL-10 between genotypes. Interestingly, blockade of glycolysis using 2-deoxyglucose (2DG) led to a significant reduction of IL-10 in engulfed macrophages in both mouse genotypes (**Figure 7F**), suggesting that glycolysis plays an unappreciated role in AC-induced IL-10 production. More interestingly, blockade of glycolysis normalized the differential IL-10 secretion between genotypes. Next, we examined mitochondrial respiration and glycolysis by measuring OCR and ECAR, respectively. We found that ACs

decreased mitochondrial OXPHOS when engulfed by macrophages regardless of genotypes, as shown by decreased maximal respiration without significant changes in basal respiration (**Figure 7G** and **7H**). Furthermore, ACs promoted aerobic glycolysis in WT macrophages, and SLC37A2 deletion impaired AC-induced glycolysis (**Figure 7I** and **7J)**. No genotypic difference in glycolytic capacity was observed in AC-engulfed macrophages. Taken together, our results suggest that SLC37A2 positively regulates M2 (AC) activation through modulation of glycolysis and is likely independent of phagocytosis or fatty acid oxidation.

Discussion

Atherosclerosis is a chronic, low-grade inflammatory condition triggered by abnormal lipid metabolism (2-7). Our published work shows that as an ER-membrane anchored G6P transporter, SLC37A2 is a critical regulator of LPS-induced M1 macrophage activation by modulation of glycolysis (25). In the current study, we made novel observations that SLC37A2 is required for normal activation and function of M2 macrophages *in vitro,* and hematopoietic expression of SLC37A2 is atheroprotective *in vivo* under pro-atherogenic conditions. Disruption of SLC37A2 significantly impairs M2 macrophage activation induced by IL-4 or apoptotic cells. Moreover, disruption of SLC37A2 in hematopoietic cells elevates plasma and liver lipids, impairs anti-inflammatory responses, and worsens atherogenesis in high-fat western diet-fed $Ldlr^{-/-}$ mice. Since LPS, oxLDL, and IL-4 induce macrophage SLC37A2 protein expression, we speculate that induction of macrophage SLC37A2 expression promotes inflammation resolution and prevents or slows atherosclerosis progression.

Cellular metabolism has emerged as an essential determinant of macrophage activation in response to microenvironmental cues. M1 macrophage activation was long thought to primarily rely on glucose metabolism, whereas M2 (M(IL-4)) macrophages switch to fatty acid oxidation and mitochondrial biogenesis to support their anti-inflammatory functions (34). However, recent studies challenged this concept and suggested that fatty acid oxidation is dispensable for M2 (IL-4) macrophage polarization (40, 41). Whether glycolysis plays a role in M2 activation is also under debate and requires further investigation (36). Although much evidence suggests that mitochondrial OXPHOS supports M2 (IL-4) activation, how macrophages reprogram cellular metabolism to favor M2 polarization remains poorly defined. In our study, SLC37A2 deficiency impairs IL-4-induced M2 macrophage polarization independent of PPARs and PGC1. Given that SLC37A2 regulates glycolysis and mitochondrial OXPHOS in LPS-treated macrophages, we hypothesized that SLC37A2 might promote IL-4-induced M2 activation by enhancing mitochondrial respiration. Our results showed that 24 h of IL-4 stimulation significantly increased glycolysis and mitochondrial respiration in macrophages regardless of SLC37A2 expression.

Despite the impaired M2 activation in response to IL-4, SLC37A2 deletion slightly increased mitochondrial respiration and had no effect on glycolysis in IL-4 polarized M2 macrophages. These results suggest that the impaired M2 (IL-4) activation in SLC37A2-deficient macrophages is likely regulated by unknown mechanisms rather than rewiring the glycolytic process or altering mitochondrial respiration. Additionally, mitochondrial β-oxidation of fatty acids derived from apoptosis has been shown to support IL-10 production during the process of efferocytosis (39). Interestingly, our study suggests that glycolysis plays a much greater role in AC-induced IL-10 production, as evidenced by the increased ECAR in AC-treated macrophages and a much greater reduction of IL-10 in 2DG-treated macrophages relative to etomoxir-treated cells. Our results agreed with Morioka's fininds that efferocytosis protes glycose uptake, glycolysis, and lactate production (42). Different from LPS-treated macrophages in which SLC37A2 deletion promotes glycolysis, SLC37A2-deficient macrophages showed attenuated glycolysis in response to AC stimulation. Furthermore, blockade of glycolysis, but not phagocytosis or fatty acid oxidation, normalized the differential secretion of IL-10 between genotypes. Taken together, our results suggest that glucose metabolism plays a central role in SLC37A2-regulated M2 (AC) activation.

The primary functions of M2 macrophages are to promote tissue remodeling and repair through collagen formation and engulfment and clearance of apoptotic cells (i.e., efferocytosis). Failure of efferocytosis will lead to increased apoptosis and cell death. Additionally, M2 macrophages also secrete high levels of anti-inflammatory cytokines such as IL-10 and TGF-β. IL-10 is a crucial mediator of inflammation resolution (43). It can also promote efferocytosis by a positive feedback pathway (44). Blocking IL-10 accelerates atherosclerosis (45), whereas targeting delivery of IL-10 via nanoparticles attenuates atherosclerosis (46). In our study, although no significant changes in apoptosis or efferocytosis in atherosclerotic plaques were observed between genotypes, loss of SLC37A2 in bone marrow did enlarge necrotic cores and decrease collagen deposition in the diet-fed mouse plaques. This could suggest secondary necrosis of apoptotic cells may have nonetheless occurred. Moreover, plasma IL-10, but not

plasma cholesterol, shows an inverse correlation with aortic plaque size in diet-fed mice. Taken together, our *in vivo* and *in vitro* studies consistently suggest that SLC37A2 expression is necessary for proper M2 macrophage activation. The impaired M2 responses in the hematopoietic SLC37A2-deficient mice are sufficient to drive atherosclerosis under hyperlipidemic conditions.

Our *in vitro* macrophage studies suggest that SLC37A2 deletion enhances pro-inflammatory activation in both LPS- and oxLDL-treated macrophages. However, hematopoietic SLC37A2 deletion does not cause elevated pro-inflammatory responses in WD-fed Ldlr$^{-/-}$ mice. Unexpectedly, plasma MCP-1 was significantly down-regulated in hematopoietic SLC37A2-deficient mice. MCP-1 is one of the critical chemokines that regulate the migration and infiltration of monocytes/macrophages. A higher circulating level of MCP-1 is associated with an increased long-term risk of stroke in the general population (47). Inhibition of MCP-1 (48) or its receptor CCR2 (49-51) using a genetic approach with pharmacological treatment decreases plaque size and limits macrophage infiltration in experimental models of atherosclerosis. As discussed above, hematopoietic SLC37A2 deletion increases lipid deposition and necrotic core formation but does not enhance macrophage (CD68^{+} cells) infiltration in diet-fed Ldlr$^{-/-}$ mice. One possible explanation for the indistinguishable macrophage content between genotypes is the net effect of reducing anti-inflammatory IL-10 and pro-inflammatory MCP-1 in those KO mice. Interestingly, IL-4 signaling induces MCP-1 expression in macrophages and other cells (52-54). We observed a significant decrease in MCP-1 expression induced by IL-4 in SLC37A2-deficient macrophages. Whether the down-regulation of MCP-1 expression results from the impaired IL-4 response in WD-diet fed hematopoietic SLC372 deficient mice requires further investigation. On the other hand, macrophage heterogeneity is more complex as activation drives a spectrum of macrophages (55). *In vitro* models of M1 or M2 activation of macrophages are highly simplified as compared with the microenvironment that macrophages encounter in an atherosclerotic lesion or liver tissue. The mixed pro-inflammatory and anti-inflammatory profile in diet-fed Slc37a2$^{\Delta hema}$ mice likely reflects a more complex local microenvironment that macrophages encounter in an atherosclerotic lesion or liver tissue in those diet-fed mice.

Alternative or M2 activation of hepatic macrophages promotes liver fatty acid oxidation and improves metabolic syndrome (26). One interesting observation in the current study is that the Slc37a2$^{\Delta hema}$ mice displayed increased plasma and liver cholesterol and concomitantly decreased expression of genes encoding liver fatty acid oxidation enzymes and M2 macrophage marker expression in the liver after 16-wk WD feeding. Our results suggest that SLC37A2 deletion impairs alternative activation of Kupffer cells, leading to decreased fatty acid oxidation and increased neutral lipid accumulation in the liver and plasma. Since Kupffer cell replacement in Slc37a2$^{-/-}$ BMT mice is incomplete (56), the modest elevation of plasma and liver lipids in the Slc37a2$^{\Delta hema}$ mice may underestimate the harmful effect of SLC37a2 deletion on liver lipid homeostasis in the context of atherosclerosis. The incomplete replacement of resident macrophages likely will dilute the impact of macrophage SLC37A2 deletion on atherogenesis or tissue macrophage inflammation.

In summary, under *in vivo* pro-atherogenic conditions (chronic and metabolic stress conditions), hematopoietic SLC37A2 expression is necessary for maintaining M2 macrophage activation and IL-10 production. Loss of hematopoietic SLC37A2 impairs anti-inflammatory activities at the cell (peritoneal macrophages), tissue (liver), and systemic (plasma) levels and accelerates atherosclerosis. Our study provides evidence that SLC37A2 expression in macrophages protects against atherosclerosis in mice.

Limitation of the study

One of the limitations of the BMT model is that BM contains multiple types of immune cells. Many of them, including T and B cells (57, 58), and dendritic cells (59, 60), are involved in atherogenesis. Because of this, we cannot distinguish the specific contribution of macrophage SLC37A2 from other immune cells to atherosclerosis. Additionally, in our BMT study, we only examined atherosclerosis after 16-wks diet feeding, a more advanced stage of atherosclerosis. Lastly, we only used male Ldlr$^{-/-}$ mice as recipient

mice to investigate the impact of hematopoietic SLC37A2 deficiency on the pathogenesis of atherogenesis and obesity and insulin resistance induced by high-fat western diet feeding. Therefore, we do not know whether there is a sex-dependent effect of hematopoietic SLC37A2 expression on the pathogenesis of atherogenesis or not.

Methods

Animals, bone marrow transplantation (BMT), and diet feeding

Animals: *Slc37a2* global knockout (KO) mice in the C57BL/6J background (T1837) were purchased from Deltagen, Inc (25). Heterozygous *Slc37a2* KO mice were intercrossed to obtain wild type (WT) and homozygous KO (*Slc37a2*$^{-/-}$) mice. Ldlr$^{-/-}$ (stock 002207) mice were purchased from Jackson Laboratories. Mice were housed in a pathogen-free facility on a 12 h light/dark cycle and received a standard laboratory diet.

BMT**:** BMT was performed as described before (61). Briefly, male Ldlr$^{-/-}$ recipient mice at 7 wks of age received a sublethal dose of radiation (900 rads) 4 h prior to bone marrow injection. 7×10^6 BM cells from female donor (WT and *Slc37a2*$^{-/-}$) mice were injected into the retro-orbital venous plexus of irradiated male Ldlr$^{-/-}$ recipient mice. Repopulation of blood leukocytes after BMT was evaluated after 16 wks of diet feeding by determining the percentage expression of the Y-chromosome-associated sex-determining region Y gene (Sry) in genomic DNA obtained from white blood cells, as described previously (61).

High-fat western diet (WD) feeding: After 5 wks for recovery from radiation, Ldlr$^{-/-}$ recipient mice were switched from a standard laboratory diet to a high-fat WD containing 42% calories from fat and 0.2% cholesterol (TD. 88137, Teklad) for an additional 16 wks to induce advanced atherosclerosis.

All animal experimental protocols were approved by the Wake Forest University Animal Care and Use Committee.

Analysis of atherosclerotic lesions

Aortic root atherosclerosis was assessed as described before (61). Briefly, aortic roots were embedded in Optimal Cutting Temperature (Tissue Tek) media and cut at 8 µm intervals. Sections were stained in 0.5% Oil Red O for 25 min, and counterstained with hematoxylin. Stained sections were photographed

with an Olympus DP71 digital camera and quantified using NIH ImageJ software. To measure necrosis, boundary lines were drawn using NIH ImageJ software around regions that were free of H&E staining. We used a 3000 μm^2 threshold to avoid counting regions that may not represent substantial areas of necrosis, as described before (61). Results were expressed as cross-sectional plaque area (H&E) or plaque necrosis (necrotic core), or percent of total plaque area or necrosis core.

Macrophages and T cells in aortic root were stained by incubating aortic root cross-sections with the primary antibodies to CD68 (Bio-Rad) and CD3 (Abcam), followed by the biotinylated secondary antibody. The staining was visualized using the ABC reagent (ABC vector kit; Vector) and DAB substrate chromogen (Dako). Apoptotic cells in atherosclerotic lesions were stained using the Click-iT Plus TUNEL Assay kit (Thermo Fisher) according to the manufacturer's protocol. The sections were then stained with CD68 antibody (Bio-Rad), and nuclei were stained with DAPI. Only TUNEL-positive cells that co-localized with DAPI-positive nuclei were counted as apoptotic cells. Efferocytosis was determined by counting the number of macrophage-associated versus free apoptotic cells, following established methods published before (61-65). Aortic root cross-sections were also stained with Masson's Trichrome stain to quantify collagen deposition. Areas stained blue within lesions were identified as collagen-positive using NIH ImageJ software.

Cell culture and treatment

Peritoneal macrophage culture: Resident peritoneal macrophages were harvested from mice after 16-wk diet feeding by flushing the peritoneal cavity with cold PBS (66, 67). The peritoneal cells were plated in RPMI-1640 media containing 100 U/ml penicillin and 100 µg/ml streptomycin and cultured at 37°C in a 5% CO2 incubator. After a 2 h incubation, floating cells were removed by washing with PBS, and adherent macrophages were lysed using Trizol (Invitrogen) for RNA extraction.

BMDM culture: BMDMs were cultured as described previously (25). Briefly, mouse bone marrow was cultured in low glucose Dulbecco's modified Eagle's medium (DMEM) supplemented with 30% L929 cell-conditioned medium, 20% fetal bovine serum (FBS), 2 mM L-glutamine, 1 mM sodium pyruvate, 100 U/ml penicillin, and 100 µg/ml streptomycin for 6-7 days until the cells reached confluence. BMDMs were then lifted from the dishes and incubated overnight in RPMI 1640 medium containing 1% Nutridoma-SP medium (Sigma-Aldrich, St. Louis, MO) before any treatment.

Jurkat T cell culture: Jurkat T cells (TIB-152, ATCC) were maintained in RPMI-1640 medium supplemented with 10% FBS, 2 mM L-glutamine, 1 mM sodium pyruvate, 100 U/ml penicillin, and 100 µg/ml streptomycin (RPMI-1640 complete medium) at $1x10^5$ to $1x10^6$ cells/ml. To induce apoptosis, Jurkat T cells ($2x10^6$/ml) were treated with 1 μM staurosporine in RPMI-1640 media containing 100 U/ml penicillin and 100 µg/ml streptomycin for 4 h.

Macrophage stimulation: To induce M2 macrophages activation, BMDMs were treated with murine IL-4 (PeproTech) or apoptotic cells (ACs) to induce M2a (M2 (IL-4)) or M2c (M2 (AC), respectively. Briefly, BMDMs were incubated with 20 ng/ml IL-4 or ACs (ratio of ACs to macrophages was 5:1) in RPMI-1640 medium complete medium for indicated times as written in the figure legends. To induce foam cell formation, BMDMs were treated with 25 or 50 μg/ml oxLDL (Athens Research & Techology) for 0-24 h. In some experiments, BMDMs were pretreated for 30 min with hexokinase inhibitor 2-deoxy-D-glucose (2-DG; 10 mM, Sigma-Aldrich, St. Louis, MO), actin polymerization inhibitor cytochalasin D (10 μM, Cayman), and fatty acid β-oxidation inhibitor etomoxir (50 μM, Cayman) and subsequently treated with apoptotic cells for an additional 4 h in the presence of each inhibitor.

Cytokine quantification

Total RNA in the liver, adipose tissue, peritoneal macrophages, or BMDMs was extracted using Trizol (Invitrogen). cDNA preparation and real-time PCR were conducted as described previously (25, 61). Primers used in the study were listed in Table S1. Concentrations of cytokines/chemokines in plasma, liver homogenate, or cell culture supernatant were measured using Bioplex assay or ELISA according to the manufacturer's instructions.

Flow cytometry

Peripheral blood was collected from the retro-orbital venous plexus into heparin-containing tubes. Spleen was isolated from anesthetized mice after 16-wk diet feeding, followed by mashing with a 1ml syringe plunger through a 70µm cell strainer. Filtered cells were washed twice, and the cell pellet was resuspended in staining buffer. Red blood cells in peripheral blood and splenocytes were removed by treatment with ACK lysing buffer (Gibco, cat# A10492). The remaining cells were incubated with Gr1(Ly6C/G)-PerCP-Cy5.5 (BD Pharmingen, cat# 552093), CD115-APC (eBioscience, cat# 17-1152-82), CD11b-APC Cy7 (BD Bioscience, cat#557657), and V450-CD45 (BD Horizon, cat# 560501) (66). Monocytes were identified as $CD45^{+}CD115^{+}$ and further separated into $Gr1^{high}$ and $Gr1^{low}$ subsets, and neutrophils were identified as $CD45^{+}CD115^{-}Gr1^{+}$. Data were acquired on a BD FACS Canto II instrument (BD Biosciences, Becton, Dickinson) and analyzed using FACSDiva software v6.1.3 (BD Biosciences, Becton, Dickinson). To examine the apoptotic rate after staurosporine treatment, Jurkat T cells were stained with Annexin V-APC and PI by using a Dead Cell Apoptosis Kit (ThermoFisher). Data were acquired on a BD FACSCalibur (BD Biosciences, Becton, Dickinson) and analyzed using Flowjo V7.6.5 (BD Biosciences).

Glucose tolerance tests (GTTs) and insulin tolerance tests (ITTs)

GTTs and ITTs were done after 10 wks of diet consumption. Briefly, for GTTs, mice were fasted overnight before intraperitoneal (ip) injection of 1 g glucose/kg BW. One wk later, the same groups of mice were

used for ip injection of 0.75 U of regular human insulin/kg BW after a 4 h fast. Blood glucose concentrations were measured at 0, 15, 30, 60, and 120 min after injection.

Lipid analysis

Blood samples were taken from tail veins following a 4 h fast during the light cycle before and at 4 wks intervals after WD feeding began. Plasma total cholesterol, free cholesterol (Wako), and triglyceride (TG) (Roche) were determined by enzymatic analysis according to the manufacturer's instructions. Plasma from 16-wk diet-fed mice was fractionated by FPLC to determine cholesterol distribution among the lipoprotein classes (68).

Liver lipids were extracted with chloroform: methanol (2:1), and the extract was used for enzymatic assays (cholesterol, Wako; TG, Roche). Data were normalized to wet liver weight (61). Macrophage cholesterol was extracted from BMDMs using isopropyl alcohol. Cellular total cholesterol (TC) and free cholesterol (FC) content were measured by gas-liquid chromatography (69). Lipid concentrations were normalized to macrophage protein, determined by Lowry protein assay, as described previously (69).

Seahorse assay

2 x 10^5 BMDMs were plated into each well of Seahorse XF96 cell culture microplates (Agilent Technologies, Santa Clara, CA) and cultured overnight before treated with or without 20 ng/ml IL-4 for 6 or 24 h or ACs for 3 h. Macrophages were then incubated at 37 ^{o}C for a minimum of 45 minutes in the absence of CO_2 in the Seahorse medium (pH 7.4) supplemented with 1 mM pyruvate, 2 mM L-glutamine, and 25 mM glucose for mitochondrial stress test or without glucose for glycolytic test. Basal and IL-4- or AC-induced changes in OCR and ECAR rates in BMDMs were measured with a Seahorse XF96 Extracellular Flux Analyzer (Agilent Technologies, Santa Clara, CA) under basal conditions and following the sequential addition of 10 mM glucose, 1 µM oligomycin, 1.5 µM fluoro-carbonyl cyanide phenylhydrazone (FCCP), 100 nM rotenone plus 1 µM antimycin A, and 50 mM 2DG (all the compounds

were from Agilent Technologies, Santa Clara, CA), as described in the figure legends. After the assay, 3 μM Hoechst (Life Technologies) was added to each well to stain nuclei for cell counting. Results were collected with Wave software version 2.6 (Agilent Technologies, Santa Clara, CA) and data was normalized to cell counting.

Western blotting

BMDMs were lysed in radioimmunoprecipitation assay (RIPA) buffer containing protease inhibitor cocktails and PhosSTOP (Roche). Protein concentration was measured using the BCA Protein Assay Kit (Pierce). Rabbit anti-SLC37A2 polyclonal antibody was made against the peptide CTPPRHHDDPEKEQDNPEDPVNSPYSSRES (LAMPIRE Biological Lab Inc., Everett, PA) and used at a dilution of 1:500 (25).

Statistics

Statistical analysis was performed using GraphPad Prism software 7 (GraphPad Software) except for the plasma lipid analysis in Figures 1A-1D. Data are presented as the mean ± SEM unless indicated otherwise. Differences were compared with Student's t-test or two-way ANOVA with post hoc Tukey's multiple comparison test. P values and statistical analysis are indicated in the figure legends.

In Figures 1A-1D, the mixed effects models were used to compare lipids variables between genotype groups at each time point. Use of random intercepts provided a source of autocorrelation between repeated measures. Genotype groups and weeks and the interaction between genotype groups and weeks were included in the model. Contrasts were used to compare lipid variables at each measured week. $P < 0.05$ was considered statistically significant.

Author contributions

Q.Z. performed lipid analysis, qPCR, western blotting, GTT, ITT, and *in vitro* macrophage experiments; Z. W. performed tissue histology analysis, flow cytometry assay, *in vitro* cell experiments, and helped draft the manuscript; A.K.M performed the seahorse analysis; M.Z. performed liver lipid extraction, aortic root sectioning, and helped with mouse necropsy; E. B. helped with mouse necropsy; J. M. and M. B. F. helped with multiplex assay and manuscript writing; F.C.H. helped with statistical analysis; C.E.M., C.M.F, and J.S.P. helped with manuscript writing and data discussion; X.Z. conceived the study and wrote the manuscript.

Acknowledgments

This study was supported by the Intramural Research Program of the NIEHS Z01 ES102005 (M.B.F.), NIH R01 HL119962 (J.S.P.), NIH R35 GM126922 (C.E.M.), NIH R01 HL132035 (X.Z.), NIH T32GM127261 (A.K.M.), and NIH T32 AI007401 (A.K.M.).

Figure 1

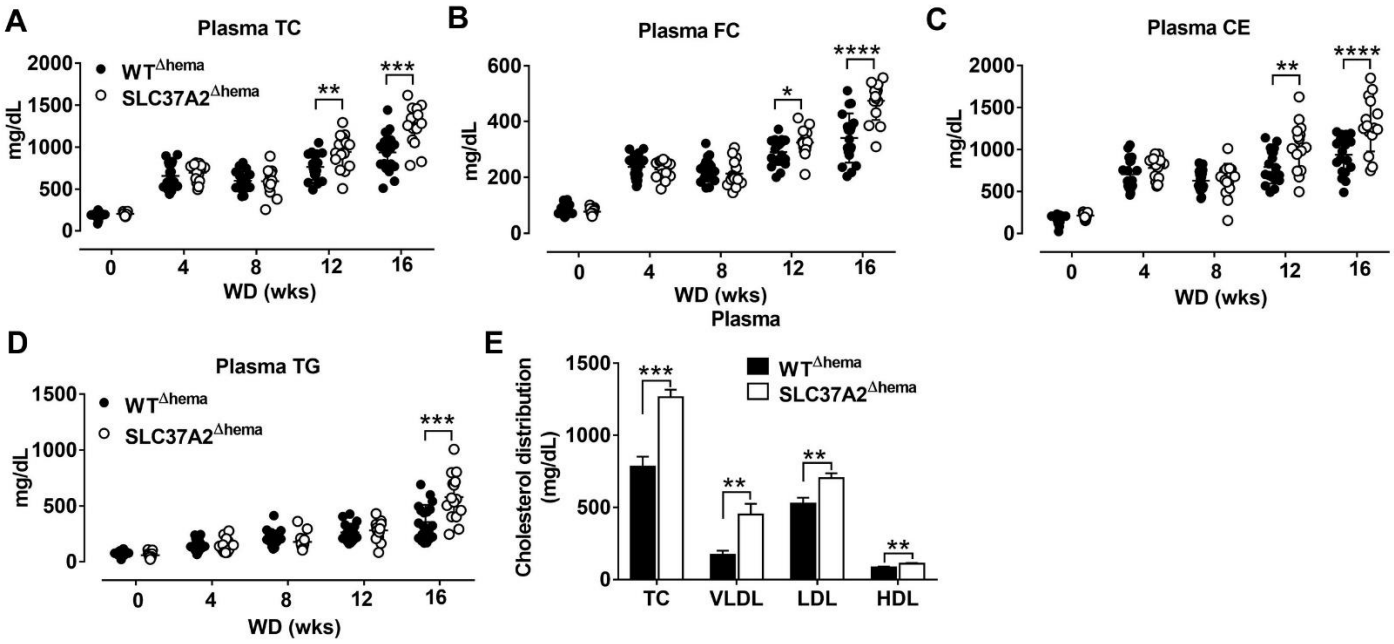

Figure 1. Hematopoietic SLC37A2 deletion increases plasma lipids in WD-fed Ldlr$^{-/-}$ mice. Hematopoietic SLC37A2 knockout (SLC37A2$^{\Delta hema}$) and control (WT$^{\Delta hema}$) Ldlr$^{-/-}$ mice were switched from a standard laboratory diet to high-fat WD for 16 wks to promote the development of advanced atherosclerosis.

(**A-D**) Fasting (4 h) plasma total cholesterol (TC), free cholesterol (FC), cholesterol ester (CE), and triglyceride (TG) concentrations were measured by enzymatic assays over time (0–16 wks) (n=12-16).

(**E**) Plasma cholesterol distribution among lipoproteins after 16 wks of WD feeding was determined after fractionation of plasma by fast protein liquid chromatography (n=6-8).

Data are expressed as mean ± SEM. ** P<0.01, *** P<0.001, **** P<0.0001, unpaired, two-tailed Student's t-test. HDL indicates high-density lipoprotein; LDL, low-density lipoprotein; and VLDL, very-LDL.

Figure 2

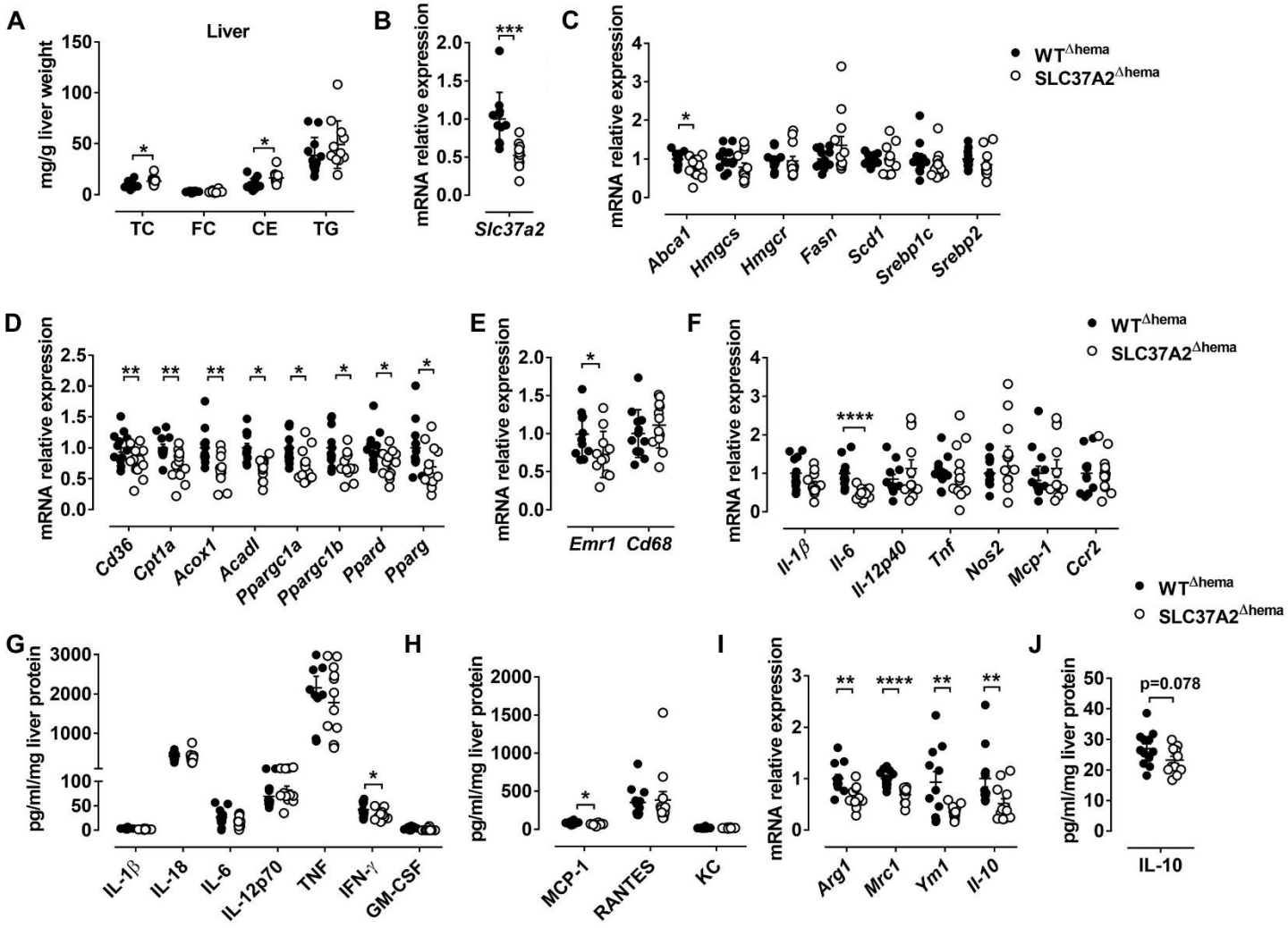

Figure 2. Hematopoietic SLC37A2 deletion increases liver CE and reduces hepatic M2 macrophage activation in WD-fed LDLrKO mice.

Irradiated Ldlr$^{-/-}$ mice transplanted with WT or SLC37A2KO bone marrow were fed a high-fat western diet for 16 wks.

(**A**) Fasting (4 h) total cholesterol (TC), free cholesterol (FC), cholesterol ester (CE), and triglyceride (TG) concentrations in the liver were measured by enzymatic assays (n=12 per genotype).

(**B**) Slc37a2 transcript expression in liver (n=12 per genotype).

(**C**) Relative transcript levels for cholesterol efflux, cholesterol synthesis, fatty acid synthesis, and transcriptional regulators controlling these pathways in the liver (n=12 per genotype).

(**D**) Relative transcript levels for genes encoding key enzymes in fatty acid uptake, β-oxidation, and transcriptional regulators controlling these pathways in the liver (n=12 per genotype).

(**E-F**) Relative transcript levels for genes encoding macrophage markers (E) and pro-inflammatory cytokines (F) in the liver (n=12 per genotype).

(**G-H**) Liver cytokine and chemokine protein concentrations (n=12 per genotype).

(**I**) Relative transcript levels for genes encoding macrophage markers (E) and pro-inflammatory cytokines (F) in the liver (n=12 per genotype).

(**J**) Liver IL-10 protein concentrations (n=12 per genotype).
Data are expressed as mean ± SEM. *** P<0.01, *** P<0.001, **** P<0.0001, unpaired, two-tailed Student's t-test.

Figure 3

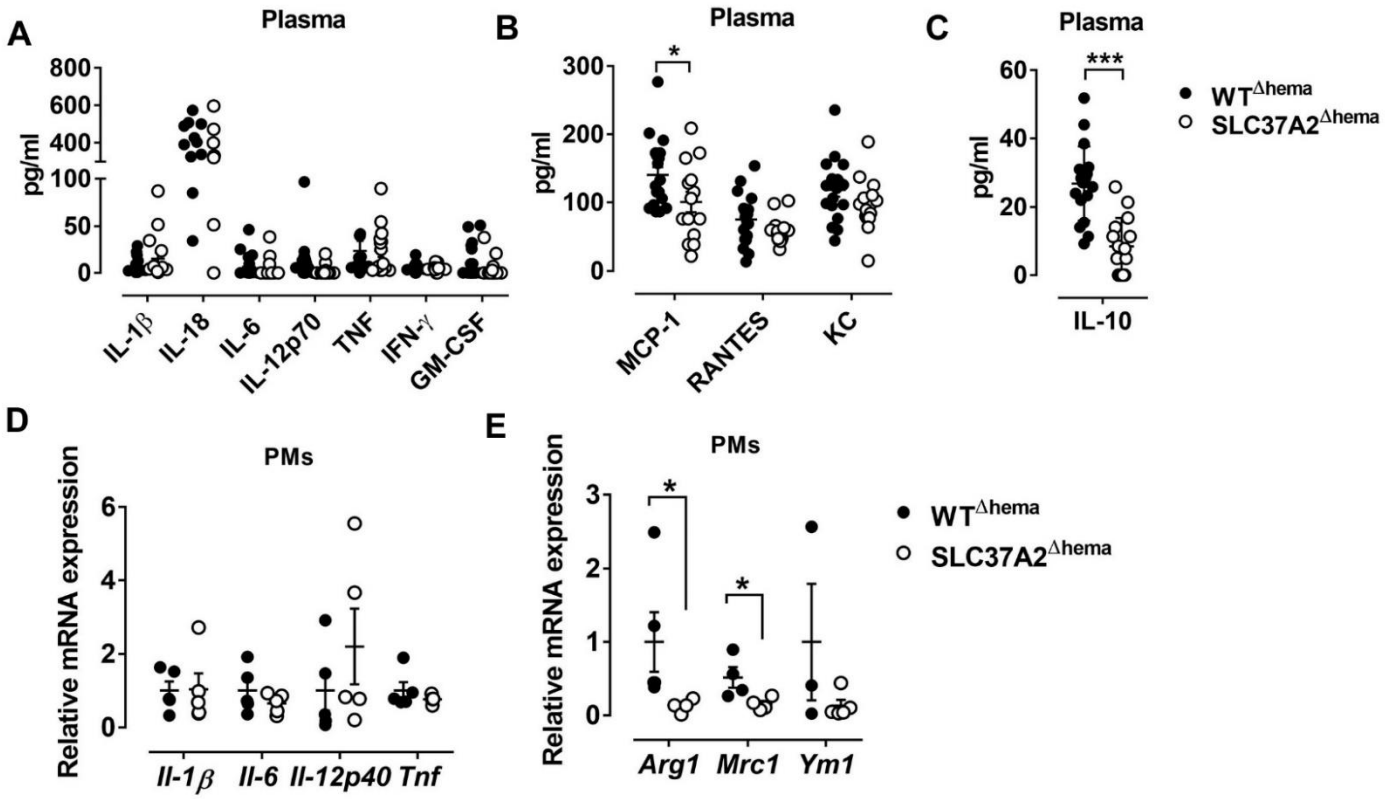

Figure 3. Hematopoietic SLC37A2 deletion impairs anti-inflammatory responses in WD-fed Ldlr$^{-/-}$ mice.

Hematopoietic SLC37A2 knockout (SLC37A2$^{\Delta hema}$) and control (WT$^{\Delta hema}$) Ldlr$^{-/-}$ mice were fed a high-fat western diet for 16 wks.

(**A-C**) Plasma pro-inflammatory cytokine (A), chemokine (B), and anti-inflammatory cytokine IL-10 (C) concentrations were quantified by multiplex assay.

(**D-E**) Relative transcript levels of M1 and M2 activation markers in resident peritoneal macrophages. Each symbol represents an individual mouse.

Data are expressed as mean ± SEM. *$p<0.05$; ***$p<0.001$, unpaired, two-tailed Student's t-test.

Figure 4

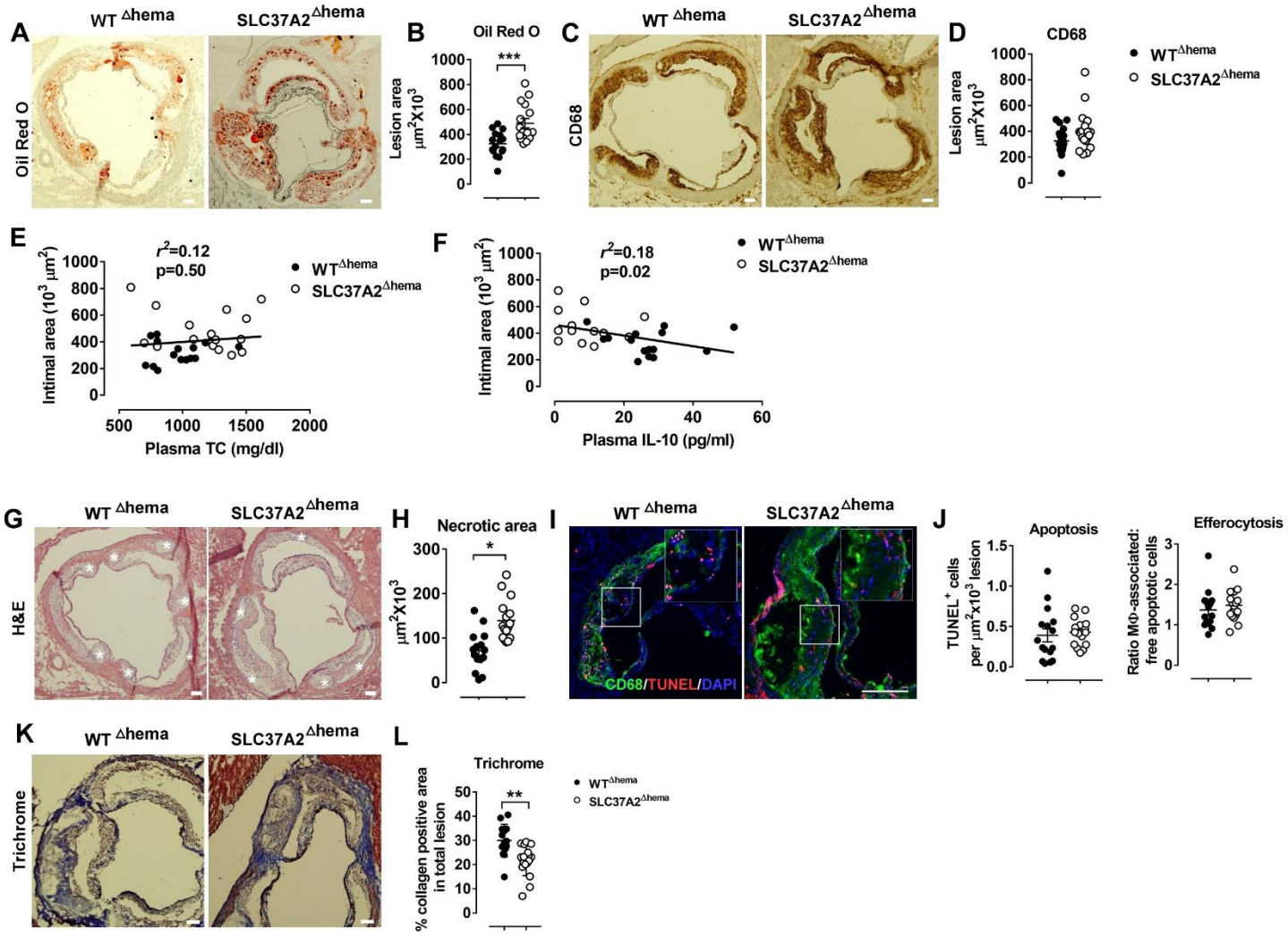

Figure 4. Hematopoietic SLC37A2 deficiency promotes atherosclerosis in WD-fed Ldlr$^{-/-}$ mice. Hematopoietic SLC37A2 knockout (SLC37A2$^{\Delta hema}$) and control (WT$^{\Delta hema}$) Ldlr$^{-/-}$ mice were fed a high-fat western diet for 16 wks (n=12-16 mice per genotype).

(**A-B**) Quantification of Oil Red O positive intimal area in the aortic root.

(**C-D**) Quantification of CD68^{+} cells (macrophages) in the aortic root intimal area.

(**E**) Linear regression analysis of aortic root intimal area vs. plasma total cholesterol of 16-wk diet-fed mice. Each point represents an individual animal of the denoted diet group and the correlation coefficient is shown for the entire data set.

(**F**) Linear regression analysis of aortic root intimal area vs. plasma IL-10 of 16-wk diet-fed mice. Each point represents an individual animal of the denoted diet group and the correlation coefficient is shown for the entire data set.

(**G-H**) Quantification of the aortic necrotic intimal area (total necrotic area) in H&E stained aortic root sections. White stars indicates necrotic area in the plaques (G).

(**I-J**) Quantification of apoptosis (TUNEL-positive cells) and efferocytosis (the ratio of macrophage-associated: free apoptotic cells) in aortic root sections. CD68 (green; macrophages), TUNEL (red), and DAPI (blue; nuclei) were labeled fluorescently.

(**K-L**) Quantification of aortic Trichrome stain positive cells.
Scale bars = 100 μm. Each symbol represents an individual mouse. Data are expressed as mean ± SEM. n = 12-16 mice per group. *$p < 0.05$; **$p < 0.01$; ***$p<0.001$.

Figure 5

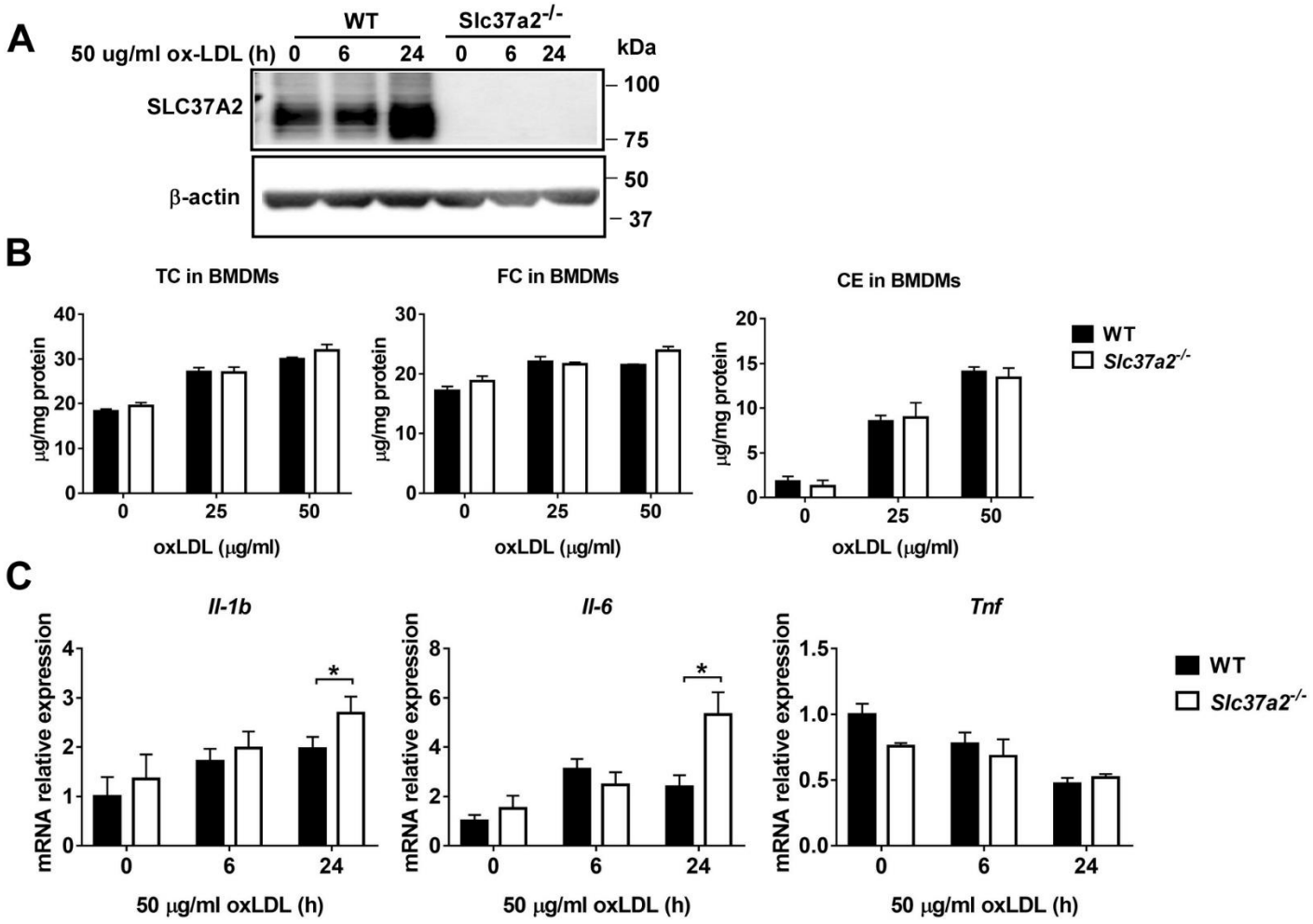

Figure 5. SLC37A2 deficiency promotes oxidized LDL (OxLDL)-induced macrophage inflammation *in vitro*.

(**A**) SLC37A2 protein expression analyzed by Western blotting in WT and *Slc37a2*$^{-/-}$ bone marrow-derived macrophages (BMDMs) treated with 50 μg/ml oxLDL for 0-24 h.

(**B**) Quantification of cellar total cholesterol (TC), free cholesterol (FC), and cholesterol ester (CE) in WT and *Slc37a2*$^{-/-}$ BMDMs after treated with or without 25 μg/ml or 50 μg/ml oxLDL for 24 h.

(**C**) Relative transcript level of cytokines in WT and *Slc37a2*$^{-/-}$ BMDMs stimulated with 50 μg/ml oxLDL for 0-24 h, measured by by qPCR.

Data are representative of two independent experiments with 3 samples per group (mean ± SEM). *$p < 0.05$; unpaired, two-tailed Student's t-test.

Figure 6

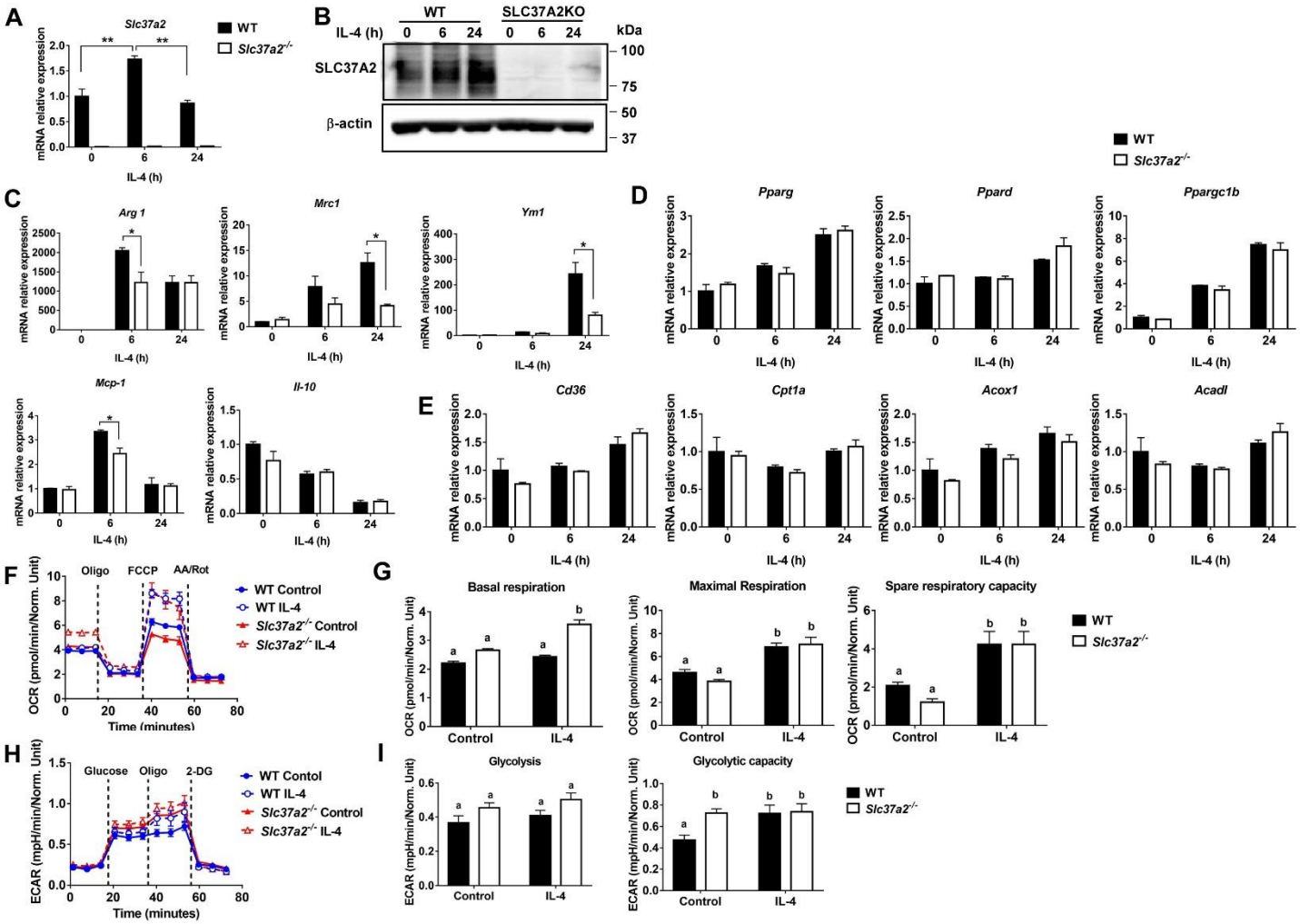

Figure 6. SLC37A2 deficiency impairs IL-4-induced M2 macrophage activation *in vitro*.
(**A-B**) SLC37A2 expression in WT and *Slc37a2*$^{-/-}$ bone marrow-derived macrophages (BMDMs) stimulated with 20 ng/ml IL-4 for 0-24 h. (A) relative transcript expression and (B) protein expression of SLC37A2 measured by qPCR and western blotting, respectively.
(**C**) Relative transcript level of M2 markers, including arginase -1 (Arg), mannose receptor, type I (Mrc1), Ym1, IL-10, and chemokine MCP-1, in WT and *Slc37a2*$^{-/-}$ BMDMs stimulated with 20 ng/ml IL-4 for 0-24 h.
(**D-E**) The relative transcript level of PPARs and genes encoding transporters or enzymes involved in fatty acid uptake or β-oxidation in WT and *Slc37a2*$^{-/-}$ BMDMs stimulated with 20 ng/ml IL-4 for 0-24 h.
(**F**) Seahorse analysis of oxygen consumption rate (OCR) in WT and *Slc37a2*$^{-/-}$ BMDMs treated with or without 20 ng/ml IL-4 for 24 h.
(**G**) Seahorse analysis of extracellular acidification rates (ECAR) in WT and *Slc37a2*$^{-/-}$ BMDMs treated with or without 20 ng/ml IL-4 for 24 h.
Data are representative of two independent experiments with 3 samples per group (mean ± SEM). *$p < 0.05$; **$p < 0.01$; unpaired, two-tailed Student's t-test (A, C, D, and E). Values with different superscripts differ significantly ($p<0.05$); two-way ANOVA with post hoc Tukey's multiple comparisons test (G and I).

Figure 7

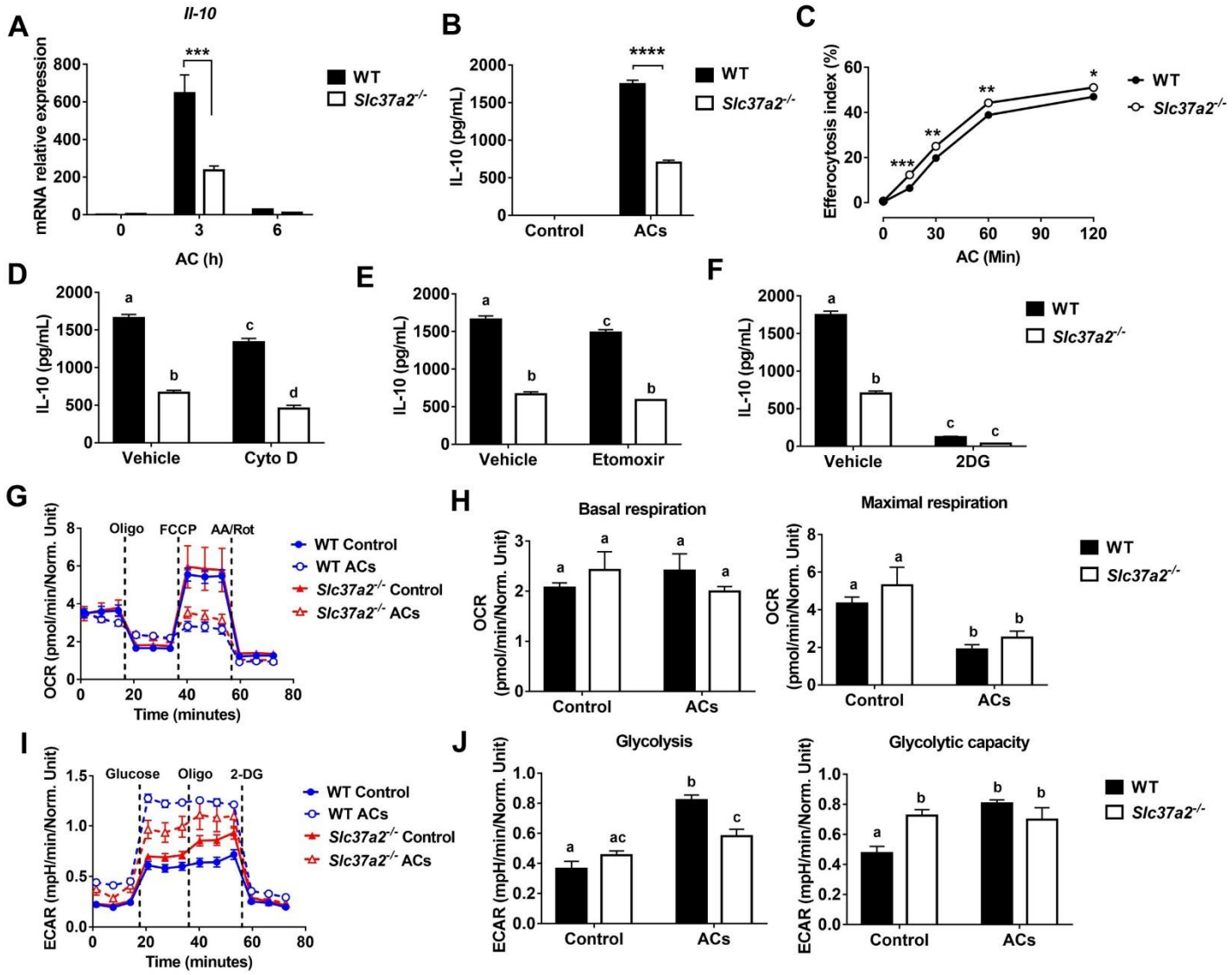

Figure 7. SLC37A2 deficiency impairs apoptotic cell-induced M2 macrophage activation *in vitro*.
(**A**) IL-10 transcript expression in WT and *Slc37a2*$^{-/-}$ BMDMs stimulated with apoptotic Jurkat T cells (ACs) (macrophages: ACs=1:5) for 0-6 h. Jurkat T cells were incubated with 1 uM staurosporine for 4 h to induce apoptosis.
(**B**) IL-10 protein secretion from WT and *Slc37a2*$^{-/-}$ BMDMs stimulated with ACs (macrophages: ACs=1:5) for 4 h.
(**C**) Efferocytosis index was measured by incubating WT and *Slc37a2*$^{-/-}$ BMDMs with ACs (macrophages: ACs =1:5) for 0-120 min. After the indicated time, macrophages were washed with cold PBS 3 times and cell dissociation buffer once before being analyzed by flow cytometry.
(**D-F**) IL-10 protein secretion from WT and *Slc37a2*$^{-/-}$ BMDMs pretreated with phagocytosis inhibitor cytochalasin D (Cyto D, 10 μM), fatty acid oxidation inhibitor etomoxir (100 μM), and hexokinase inhibitor 2-deoxy-D-glucose (2-DG; 10 mM) for 30 min, followed by co-culture with ACs (macrophages: ACs= 1:5) for 4 h.

(**G-H**) Seahorse analysis of oxygen consumption rate (OCR) in WT and *Slc37a2*$^{-/-}$ BMDMs treated with or without ACs (macrophages: ACs= 1:5) for 3 h.
(**I-J**) Seahorse analysis of extracellular acidification rates (ECAR) in WT and *Slc37a2*$^{-/-}$ BMDMs treated with or without ACs (macrophages: ACs= 1:5) for 3 h.
Data are representative of two independent experiments with 3 samples per group (mean ± SEM). ** P<0.01, *** P<0.001, **** P<0.0001, unpaired, two-tailed Student's t-test (A-C). Values with different superscripts differ significantly (p<0.05); two-way ANOVA with post hoc Tukey's multiple comparisons test (D-J).

References

1. Virani SS, Alonso A, Benjamin EJ, Bittencourt MS, Callaway CW, Carson AP, Chamberlain AM, Chang AR, Cheng S, Delling FN, et al. Heart Disease and Stroke Statistics-2020 Update: A Report From the American Heart Association. *Circulation.* 2020;141(9):e139-e596.
2. Amengual J, and Barrett TJ. Monocytes and macrophages in atherogenesis. *Current opinion in lipidology.* 2019;30(5):401-8.
3. Getz GS, and Reardon CA. Atherosclerosis: cell biology and lipoproteins. *Current opinion in lipidology.* 2020;31(5):286-90.
4. Bäck M, Yurdagul A, Jr., Tabas I, Öörni K, and Kovanen PT. Inflammation and its resolution in atherosclerosis: mediators and therapeutic opportunities. *Nature reviews Cardiology.* 2019;16(7):389-406.
5. Libby P, and Bornfeldt KE. How Far We Have Come, How Far We Have Yet to Go in Atherosclerosis Research. *Circulation research.* 2020;126(9):1107-11.
6. Flynn MC, Pernes G, Lee MKS, Nagareddy PR, and Murphy AJ. Monocytes, Macrophages, and Metabolic Disease in Atherosclerosis. *Frontiers in pharmacology.* 2019;10(666.
7. Remmerie A, and Scott CL. Macrophages and lipid metabolism. *Cellular immunology.* 2018;330(27-42.
8. Rader DJ, and Puré E. Lipoproteins, macrophage function, and atherosclerosis: beyond the foam cell? *Cell metabolism.* 2005;1(4):223-30.
9. Hansson GK, Libby P, and Tabas I. Inflammation and plaque vulnerability. *Journal of internal medicine.* 2015;278(5):483-93.
10. Yvan-Charvet L, and Ivanov S. Metabolic Reprogramming of Macrophages in Atherosclerosis: Is It All about Cholesterol? *Journal of lipid and atherosclerosis.* 2020;9(2):231-42.
11. Koelwyn GJ, Corr EM, Erbay E, and Moore KJ. Regulation of macrophage immunometabolism in atherosclerosis. *Nature immunology.* 2018;19(6):526-37.

12. Robbins CS, Hilgendorf I, Weber GF, Theurl I, Iwamoto Y, Figueiredo JL, Gorbatov R, Sukhova GK, Gerhardt LM, Smyth D, et al. Local proliferation dominates lesional macrophage accumulation in atherosclerosis. *Nature medicine.* 2013;19(9):1166-72.

13. Wang Y, Zhao M, Liu S, Guo J, Lu Y, Cheng J, and Liu J. Macrophage-derived extracellular vesicles: diverse mediators of pathology and therapeutics in multiple diseases. *Cell death & disease.* 2020;11(10):924.

14. Moore KJ, Sheedy FJ, and Fisher EA. Macrophages in atherosclerosis: a dynamic balance. *Nature reviews Immunology.* 2013;13(10):709-21.

15. Stremmel C, Stark K, and Schulz C. Heterogeneity of Macrophages in Atherosclerosis. *Thrombosis and haemostasis.* 2019;119(8):1237-46.

16. O'Neill LA, Kishton RJ, and Rathmell J. A guide to immunometabolism for immunologists. *Nature reviews Immunology.* 2016;16(9):553-65.

17. O'Neill LA, and Pearce EJ. Immunometabolism governs dendritic cell and macrophage function. *The Journal of experimental medicine.* 2016;213(1):15-23.

18. Pearce EL, and Pearce EJ. Metabolic pathways in immune cell activation and quiescence. *Immunity.* 2013;38(4):633-43.

19. Rudd JH, Warburton EA, Fryer TD, Jones HA, Clark JC, Antoun N, Johnström P, Davenport AP, Kirkpatrick PJ, Arch BN, et al. Imaging atherosclerotic plaque inflammation with [18F]-fluorodeoxyglucose positron emission tomography. *Circulation.* 2002;105(23):2708-11.

20. Freemerman AJ, Zhao L, Pingili AK, Teng B, Cozzo AJ, Fuller AM, Johnson AR, Milner JJ, Lim MF, Galanko JA, et al. Myeloid Slc2a1-Deficient Murine Model Revealed Macrophage Activation and Metabolic Phenotype Are Fueled by GLUT1. *Journal of immunology (Baltimore, Md : 1950).* 2019;202(4):1265-86.

21. Nishizawa T, Kanter JE, Kramer F, Barnhart S, Shen X, Vivekanandan-Giri A, Wall VZ, Kowitz J, Devaraj S, O'Brien KD, et al. Testing the role of myeloid cell glucose flux in inflammation and atherosclerosis. *Cell reports.* 2014;7(2):356-65.

22. Chou JY, Sik Jun H, and Mansfield BC. The SLC37 family of phosphate-linked sugar phosphate antiporters. *Molecular aspects of medicine.* 2013;34(2-3):601-11.

23. Kim JY, Tillison K, Zhou S, Wu Y, and Smas CM. The major facilitator superfamily member Slc37a2 is a novel macrophage- specific gene selectively expressed in obese white adipose tissue. *American journal of physiology Endocrinology and metabolism.* 2007;293(1):E110-20.

24. Pan CJ, Chen SY, Jun HS, Lin SR, Mansfield BC, and Chou JY. SLC37A1 and SLC37A2 are phosphate-linked, glucose-6-phosphate antiporters. *PloS one.* 2011;6(9):e23157.

25. Wang Z, Zhao Q, Nie Y, Yu Y, Misra BB, Zabalawi M, Chou JW, Key CC, Molina AJ, Quinn MA, et al. Solute Carrier Family 37 Member 2 (SLC37A2) Negatively Regulates Murine Macrophage Inflammation by Controlling Glycolysis. *iScience.* 2020;23(5):101125.

26. Odegaard JI, Ricardo-Gonzalez RR, Red Eagle A, Vats D, Morel CR, Goforth MH, Subramanian V, Mukundan L, Ferrante AW, and Chawla A. Alternative M2 activation of Kupffer cells by PPARdelta ameliorates obesity-induced insulin resistance. *Cell metabolism.* 2008;7(6):496-507.

27. Xu W, Roos A, Schlagwein N, Woltman AM, Daha MR, and van Kooten C. IL-10-producing macrophages preferentially clear early apoptotic cells. *Blood.* 2006;107(12):4930-7.

28. Tabas I. Macrophage death and defective inflammation resolution in atherosclerosis. *Nature reviews Immunology.* 2010;10(1):36-46.

29. Poon IK, Lucas CD, Rossi AG, and Ravichandran KS. Apoptotic cell clearance: basic biology and therapeutic potential. *Nature reviews Immunology.* 2014;14(3):166-80.

30. Deguchi JO, Aikawa E, Libby P, Vachon JR, Inada M, Krane SM, Whittaker P, and Aikawa M. Matrix metalloproteinase-13/collagenase-3 deletion promotes collagen accumulation and organization in mouse atherosclerotic plaques. *Circulation.* 2005;112(17):2708-15.

31. Rekhter MD. Collagen synthesis in atherosclerosis: too much and not enough. *Cardiovascular research.* 1999;41(2):376-84.

32. Libby P, Ridker PM, and Hansson GK. Progress and challenges in translating the biology of atherosclerosis. *Nature.* 2011;473(7347):317-25.

33. Maiolino G, Rossitto G, Caielli P, Bisogni V, Rossi GP, and Calò LA. The role of oxidized low-density lipoproteins in atherosclerosis: the myths and the facts. *Mediators of inflammation.* 2013;2013(714653.

34. Vats D, Mukundan L, Odegaard JI, Zhang L, Smith KL, Morel CR, Wagner RA, Greaves DR, Murray PJ, and Chawla A. Oxidative metabolism and PGC-1beta attenuate macrophage-mediated inflammation. *Cell metabolism.* 2006;4(1):13-24.

35. Chawla A. Control of macrophage activation and function by PPARs. *Circulation research.* 2010;106(10):1559-69.

36. Huang SC, Smith AM, Everts B, Colonna M, Pearce EL, Schilling JD, and Pearce EJ. Metabolic Reprogramming Mediated by the mTORC2-IRF4 Signaling Axis Is Essential for Macrophage Alternative Activation. *Immunity.* 2016;45(4):817-30.

37. Wang F, Zhang S, Vuckovic I, Jeon R, Lerman A, Folmes CD, Dzeja PP, and Herrmann J. Glycolytic Stimulation Is Not a Requirement for M2 Macrophage Differentiation. *Cell metabolism.* 2018;28(3):463-75.e4.

38. Chung EY, Liu J, Homma Y, Zhang Y, Brendolan A, Saggese M, Han J, Silverstein R, Selleri L, and Ma X. Interleukin-10 expression in macrophages during phagocytosis of apoptotic cells is mediated by homeodomain proteins Pbx1 and Prep-1. *Immunity.* 2007;27(6):952-64.

39. Zhang S, Weinberg S, DeBerge M, Gainullina A, Schipma M, Kinchen JM, Ben-Sahra I, Gius DR, Yvan-Charvet L, Chandel NS, et al. Efferocytosis Fuels Requirements of Fatty Acid Oxidation and the Electron Transport Chain to Polarize Macrophages for Tissue Repair. *Cell metabolism.* 2019;29(2):443-56.e5.

40. Divakaruni AS, Hsieh WY, Minarrieta L, Duong TN, Kim KKO, Desousa BR, Andreyev AY, Bowman CE, Caradonna K, Dranka BP, et al. Etomoxir Inhibits Macrophage Polarization by Disrupting CoA Homeostasis. *Cell metabolism.* 2018;28(3):490-503.e7.

41. Van den Bossche J, and van der Windt GJW. Fatty Acid Oxidation in Macrophages and T Cells: Time for Reassessment? *Cell metabolism.* 2018;28(4):538-40.

42. Morioka S, Perry JSA, Raymond MH, Medina CB, Zhu Y, Zhao L, Serbulea V, Onengut-Gumuscu S, Leitinger N, Kucenas S, et al. Efferocytosis induces a novel SLC program to promote glucose uptake and lactate release. *Nature.* 2018;563(7733):714-8.

43. Saraiva M, Vieira P, and O'Garra A. Biology and therapeutic potential of interleukin-10. *The Journal of experimental medicine.* 2020;217(1).

44. Ogden CA, Pound JD, Batth BK, Owens S, Johannessen I, Wood K, and Gregory CD. Enhanced apoptotic cell clearance capacity and B cell survival factor production by IL-10-activated macrophages: implications for Burkitt's lymphoma. *Journal of immunology (Baltimore, Md : 1950).* 2005;174(5):3015-23.

45. Caligiuri G, Rudling M, Ollivier V, Jacob MP, Michel JB, Hansson GK, and Nicoletti A. Interleukin-10 deficiency increases atherosclerosis, thrombosis, and low-density lipoproteins in apolipoprotein E knockout mice. *Molecular medicine (Cambridge, Mass).* 2003;9(1-2):10-7.

46. Kamaly N, Fredman G, Fojas JJ, Subramanian M, Choi WI, Zepeda K, Vilos C, Yu M, Gadde S, Wu J, et al. Targeted Interleukin-10 Nanotherapeutics Developed with a Microfluidic Chip Enhance Resolution of Inflammation in Advanced Atherosclerosis. *ACS nano.* 2016;10(5):5280-92.

47. Georgakis MK, Malik R, Björkbacka H, Pana TA, Demissie S, Ayers C, Elhadad MA, Fornage M, Beiser AS, Benjamin EJ, et al. Circulating Monocyte Chemoattractant Protein-1 and Risk of Stroke: Meta-Analysis of Population-Based Studies Involving 17 180 Individuals. *Circulation research.* 2019;125(8):773-82.

48. Gu L, Okada Y, Clinton SK, Gerard C, Sukhova GK, Libby P, and Rollins BJ. Absence of monocyte chemoattractant protein-1 reduces atherosclerosis in low density lipoprotein receptor-deficient mice. *Molecular cell.* 1998;2(2):275-81.

49. Boring L, Gosling J, Cleary M, and Charo IF. Decreased lesion formation in CCR2-/- mice reveals a role for chemokines in the initiation of atherosclerosis. *Nature.* 1998;394(6696):894-7.

50. Bot I, Ortiz Zacarías NV, de Witte WE, de Vries H, van Santbrink PJ, van der Velden D, Kröner MJ, van der Berg DJ, Stamos D, de Lange EC, et al. A novel CCR2 antagonist inhibits atherogenesis in apoE deficient mice by achieving high receptor occupancy. *Scientific reports.* 2017;7(1):52.

51. Winter C, Silvestre-Roig C, Ortega-Gomez A, Lemnitzer P, Poelman H, Schumski A, Winter J, Drechsler M, de Jong R, Immler R, et al. Chrono-pharmacological Targeting of the CCL2-CCR2 Axis Ameliorates Atherosclerosis. *Cell metabolism.* 2018;28(1):175-82.e5.

52. Rollins BJ, and Pober JS. Interleukin-4 induces the synthesis and secretion of MCP-1/JE by human endothelial cells. *The American journal of pathology.* 1991;138(6):1315-9.

53. Kikuchi H, Hanazawa S, Takeshita A, Nakada Y, Yamashita Y, and Kitano S. Interleukin-4 acts as a potent stimulator for expression of monocyte chemoattractant JE/MCP-1 in mouse peritoneal macrophages. *Biochemical and biophysical research communications.* 1994;203(1):562-9.

54. Ovsiy I, Riabov V, Manousaridis I, Michel J, Moganti K, Yin S, Liu T, Sticht C, Kremmer E, Harmsen MC, et al. IL-4 driven transcription factor FoxQ1 is expressed by monocytes in atopic dermatitis and stimulates monocyte migration. *Scientific reports.* 2017;7(1):16847.

55. Xue J, Schmidt SV, Sander J, Draffehn A, Krebs W, Quester I, De Nardo D, Gohel TD, Emde M, Schmidleithner L, et al. Transcriptome-based network analysis reveals a spectrum model of human macrophage activation. *Immunity.* 2014;40(2):274-88.

56. Kennedy DW, and Abkowitz JL. Kinetics of central nervous system microglial and macrophage engraftment: analysis using a transgenic bone marrow transplantation model. *Blood.* 1997;90(3):986-93.

57. Zhou X, Nicoletti A, Elhage R, and Hansson GK. Transfer of CD4(+) T cells aggravates atherosclerosis in immunodeficient apolipoprotein E knockout mice. *Circulation.* 2000;102(24):2919-22.

58. Zhou X, Robertson AK, Hjerpe C, and Hansson GK. Adoptive transfer of CD4+ T cells reactive to modified low-density lipoprotein aggravates atherosclerosis. *Arteriosclerosis, thrombosis, and vascular biology.* 2006;26(4):864-70.

59. Yilmaz A, Lochno M, Traeg F, Cicha I, Reiss C, Stumpf C, Raaz D, Anger T, Amann K, Probst T, et al. Emergence of dendritic cells in rupture-prone regions of vulnerable carotid plaques. *Atherosclerosis.* 2004;176(1):101-10.

60. Sun L, Zhang W, Zhao Y, Wang F, Liu S, Liu L, Zhao L, Lu W, Li M, and Xu Y. Dendritic Cells and T Cells, Partners in Atherogenesis and the Translating Road Ahead. *Frontiers in immunology.* 2020;11(1456.

61. Wang Z, Sequeira RC, Zabalawi M, Madenspacher J, Boudyguina E, Ou T, Nelson JM, Nie Y, Zhao Q, Fessler MB, et al. Myeloid atg5 deletion impairs n-3 PUFA-mediated atheroprotection. *Atherosclerosis.* 2020.

62. Thorp E, Cui D, Schrijvers DM, Kuriakose G, and Tabas I. Mertk receptor mutation reduces efferocytosis efficiency and promotes apoptotic cell accumulation and plaque necrosis in atherosclerotic lesions of apoe-/- mice. *Arterioscler Thromb Vasc Biol.* 2008;28(8):1421-8.

63. Li S, Sun Y, Liang CP, Thorp EB, Han S, Jehle AW, Saraswathi V, Pridgen B, Kanter JE, Li R, et al. Defective phagocytosis of apoptotic cells by macrophages in atherosclerotic lesions of ob/ob mice and reversal by a fish oil diet. *Circulation research.* 2009;105(11):1072-82.

64. Liao X, Sluimer JC, Wang Y, Subramanian M, Brown K, Pattison JS, Robbins J, Martinez J, and Tabas I. Macrophage autophagy plays a protective role in advanced atherosclerosis. *Cell metabolism.* 2012;15(4):545-53.

65. Schrijvers DM, De Meyer GR, Kockx MM, Herman AG, and Martinet W. Phagocytosis of apoptotic cells by macrophages is impaired in atherosclerosis. *Arteriosclerosis, thrombosis, and vascular biology.* 2005;25(6):1256-61.

66. Shen L, Yang Y, Ou T, Key CC, Tong SH, Sequeira RC, Nelson JM, Nie Y, Wang Z, Boudyguina E, et al. Dietary PUFAs attenuate NLRP3 inflammasome activation via enhancing macrophage autophagy. *Journal of lipid research.* 2017;58(9):1808-21.

67. Zhu X, Chung S, Bi X, Chuang CC, Brown AL, Liu M, Seo J, Cuffe H, Gebre AK, Boudyguina E, et al. Myeloid cell-specific ABCA1 deletion does not worsen insulin resistance in HF diet-induced or genetically obese mouse models. *Journal of lipid research.* 2013;54(10):2708-17.

68. Bi X, Zhu X, Gao C, Shewale S, Cao Q, Liu M, Boudyguina E, Gebre AK, Wilson MD, Brown AL, et al. Myeloid cell-specific ATP-binding cassette transporter A1 deletion has minimal impact on atherogenesis in atherogenic diet-fed low-density lipoprotein receptor knockout mice. *Arteriosclerosis, thrombosis, and vascular biology.* 2014;34(9):1888-99.

69. Zhu X, Lee JY, Timmins JM, Brown JM, Boudyguina E, Mulya A, Gebre AK, Willingham MC, Hiltbold EM, Mishra N, et al. Increased cellular free cholesterol in macrophage-specific Abca1 knock-out mice enhances pro-inflammatory response of macrophages. *The Journal of biological chemistry.* 2008;283(34):22930-41.